Hindawi
Advances in Civil Engineering
Volume 2018, Article ID 8658501, 8 pages
https://doi.org/10.1155/2018/8658501

Research Article

Critical Length and Collapse of Interlayer in Rock Salt Natural Gas Storage

Yingjie Wang [1] **and Jianjun Liu** [1,2]

[1] *School of Geoscience and Technology, Southwest Petroleum University, Chengdu, China*
[2] *State Key Laboratory of Geomechanics and Geotechnical Engineering, Institute of Rock & Soil Mechanics, Chinese Academy of Sciences, Wuhan, China*

Correspondence should be addressed to Jianjun Liu; jjliu@whrsm.ac.cn

Received 8 March 2018; Revised 27 June 2018; Accepted 5 July 2018; Published 2 September 2018

Academic Editor: Fengqiang Gong

The existence of an interlayer has a significant effect on the stability of a rock salt gas storage cavity; therefore, an uncontrollable collapse of the interlayer would cause a series of issues. In this study, three types of mechanical instability criteria are comprehensively calculated. The limit radius of the interlayer is computed under different criteria, and the collapse radius of the interlayer is obtained by comparison. The calculation results of the mathematical model are highly accurate with respect to actual engineering logging data, in general with over 90% of accuracy. It is demonstrated that, besides the physical and mechanical characteristics of the sandwich, the location of the interlayer in the cavity and concentration of the brine also have an important effect on the collapse of the interlayer. The brine at the bottom of the cavity is nearly saturated. Therefore, an interlayer at this location does not easily collapse. The mathematical model established in this study is used in the seismic design and prediction of interlayer collapse during the construction of salt-cavern gas storage facilities in China.

1. Introduction

The solution mining technology of injecting water to the salt bed, dissolving the rock salt, and pumping brine is the most common approach to create underground gas storage. In the process of solution mining of a salt cavern, the soft interlayer would rapidly collapse with the dissolution of the surrounding rock salt, forming a mound at the bottom. In comparison, the hard interlayer would acquire the status of a cantilever owing to its high insoluble content and hardness. Thus, preventing the continuity of the cavity walls and reducing the rate of solution mining have a tremendous effect on the shape and volume of the salt cavity [1–4]. The basic construction situation of gas storage cavern in interlayers salt rock is shown in Figure 1. In recent years, instability of the interlayer in rock salt-cavern gas storage has occurred frequently at home and abroad. There are frequent accidents such as leakage of the gas storage, destruction of the gas storage, and subsidence or collapse of the surface, which have caused great economic loss and environmental damage. In addition, the instability and collapse of the hard interlayer can also cause damage to the tube and loss of the cavity volume [5, 6].

Recently, the most common method to model an interlayer is the slab model, and numerous mechanical mechanisms for the interlayer collapse have been proposed [7–11]. Li et al. analyzed the mechanical mechanism of interlayer instability based on the critical radial stress and circular plate radial buckling and summarized the form of the interlayer collapse into two categories: insufficient strength and stability failure [12]. Jiang et al. researched the interlayer stability of the single rock salt-cavity roof using a clamped circular plate mutation model and determined the necessary condition for the instability of the rock salt-cavity roof strata [13]. Bekendam and Paar analyzed the deflection and radial stress of the roof interlayer in a single cavity and predicted the collapse of the interlayer based on the tensile strength [14]. Shi et al. solved the equilibrium differential equation corresponding to the interlayer level of radial pressure and vertical

pressure using a circular plate model and obtained the mezzanine deflection and curvature of the solution [15]. Liang et al. proposed the principle for determining the limit operating pressure of the bedded rock salt gas storage after an analysis of the characteristics of the rock salt mechanics principle, primarily including the cavity roof stability and creep deformation control of the surrounding rock [16, 17].

According to the actual construction of gas storage caverns in China, the problem of interlayer stability in the entire process of solution mining and in the operation period involves complex mechanical and technical issues, among which the mechanical problem needs to be resolved urgently [18]. Therefore, it has a very positive relevance in the study of the interlayer in solution mining and in the analysis of the effect of the interlayer on the stability of a gas storage cavern.

In this study, a mathematical model of the critical radius of an interlayer is proposed and compared with an actual rock salt interlayer collapse. The results show that the mathematical model is in strong agreement with the actual scenario and can be used as the basis for determining the interlayer collapse in a salt-cavity gas storage.

2. Mathematical Model of Interlayer

2.1. Stress Analysis of Interlayer. Owing to the strong probability of rock salt deformation, the initial stress state of a deep rock salt mine is generally under hydrostatic pressure [19, 20]. The initial geostress of an interlayer can be calculated by the following formula:

$$\sigma_{\mathrm{h}} = \sigma_{\mathrm{v}} = -\gamma_0 H = -\sum_{i=1}^{n} \gamma_i h_i, \tag{1}$$

where σ_{h} is the horizontal geostress, σ_{v} is the vertical crustal stress, γ_0 is the average unit weight, H is the depth of the interlayer, n is the number of interlayers above the depth of H, and γ_i and h_i are the unit weight and thickness of the interlayer on layer i; it is specified that the compressive stress is negative.

The interlayer in a cavity can be simplified as a fixed circular thin plate, and thus, the salt cavity can be treated as an axial-symmetric sphere. The stress on the interlayer is shown in Figure 2, where d is the diameter and t is the thickness of the interlayer. In addition, the borehole diameter is usually 224.5 mm, which can be ignored if the exposure length of the sandwich is approximately 40–60 m.

The difference between the vertical load on both sides of the sandwich is

$$q = \gamma_{\mathrm{m}} t + P_{\mathrm{t}} - P_{\mathrm{b}} = (\gamma_{\mathrm{m}} - \gamma_{\mathrm{b}}) t, \tag{2}$$

where γ_{m} is the unit weight of the interlayer; t is the thickness of the interlayer; γ_{b} is the unit weight of brine; P_{t} is the brine pressure on the top surface of the interlayer, and the value of P_{t} is $\gamma_{\mathrm{b}}(H - (t/2))$; and P_{b} is the brine pressure on the bottom surface of the interlayer, and the value of P_{b} is $\gamma_{\mathrm{b}}(H + (t/2))$.

The value of the radial pressure on the edge of the interlayer can be described by the following formula:

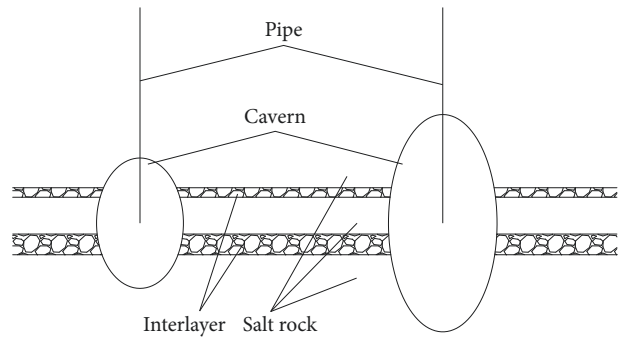

Figure 1: Schematic diagram of salt rock underground natural gas storage.

$$P_{\mathrm{r}} = M \gamma_0 H, \tag{3}$$

where M, which is called the radial pressure coefficient, is the ratio of radial pressure on the edge of the interlayer to initial stress.

The factors of the radial pressure coefficient M are sandwich depth H, interlayer length d, cavity height h, height position of the interlayer in the salt chamber η (the ratio of the distance from the sandwich to the bottom of the cavity to the height of the salt chamber), thickness of the interlayer t, elastic modulus E of the interlayer, elastic modulus E' of the interlayer socked in brine, and elastic modulus of the rock salt E_{s}. E' is equal to E at the start and less than E after the interlayer is softened. In addition, ν is not considered when the change interval is small.

The effect of each parameter on the radial pressure coefficient is set for the numerical experiment. The contents of the experimental scheme are listed in Table 1.

The radial pressure coefficient obtained from the test is listed in Table 2, where the last column indicates the coefficient of variation of the radial pressure coefficient in each set of experiments. A large coefficient of variation implies a high degree of dispersion of the data [21–23] and, consequently, a strong effect of the factors on the radial pressure coefficient.

It can be seen from Tables 1 and 2 that the radial pressure coefficient M is mainly related to the thickness of the sandwich layer t and the ratios of the elastic modulus E/E_{s} and E'/E.

The radial pressure coefficient is obtained from the three main factors derived from the test results of the numerical calculation experiment as

$$M = 1 - \frac{E'}{E} + \frac{E'}{E} 0.7333 e^{3.523/(t+4.743)} e^{0.1250 E/E_{\mathrm{s}}}. \tag{4}$$

The fitting effect based on Equation (4) is shown in Figure 3.

It can be found from the numerical experiments that a large interlayer thickness implies a small radial pressure coefficient, a large elastic modulus of the interlayer corresponds to a large radial pressure coefficient, and the radial pressure coefficient decreases linearly with the decrease in the elastic modulus of the interlayer and finally converges to 1.

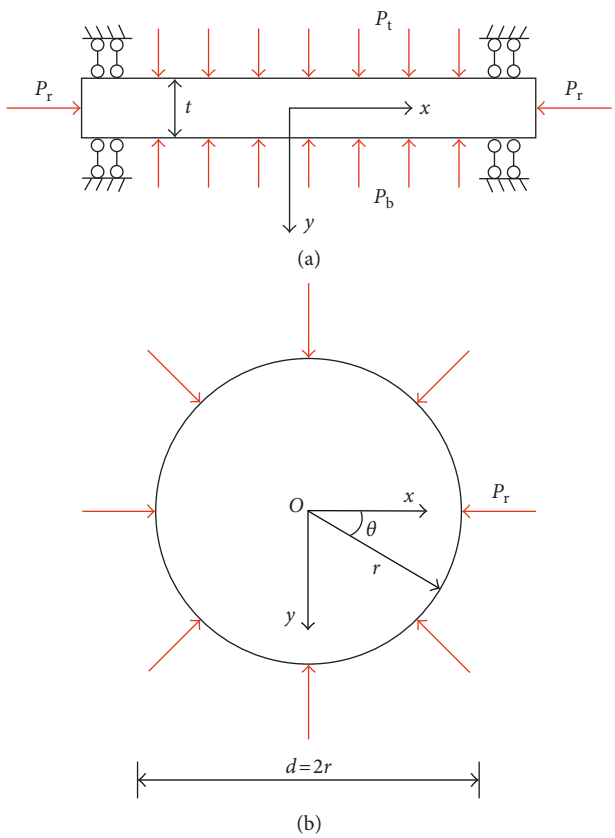

Figure 2: Force analysis of the interlayer. (a) Vertical load. (b) Horizontal load.

2.2. Deformation and Stress Distribution of Interlayer. There are two types of loading in the salt chamber: radial pressure P_r and brine pressure $\gamma_b H$ resulting in the sandwich pressure and vertical load q resulting in sandwich bending. Therefore, the stress of the interlayer is expressed as follows, based on the principle of superposition:

$$\{\sigma\} = \{\sigma\}^{(i)} + \{\sigma\}^{(ii)}, \tag{5}$$

where $\{\sigma\}$ is the stress of the interlayer, $\{\sigma\}^{(i)}$ is the compressive stress caused by the radial pressure and brine at the edge of the interlayer, and $\{\sigma\}^{(ii)}$ is the bending stress caused by the vertical uniform load q.

In a cylindrical coordinate system, $\{\sigma\}^{(i)}$ is

$$\begin{aligned} \sigma_r^{(i)} &= \sigma_\theta^{(i)} = -M\gamma_0 H, \\ \sigma_z^{(i)} &= -\gamma_b H. \end{aligned} \tag{6}$$

The interlayer can be considered as a small deflection of the circular thin bending plate when the thickness and deflection of the interlayer are small, i.e.,

$$t \le \frac{a}{5}, \tag{7}$$

Table 1: Values of each parameter.

Number	Factor (unit)	Value				
1	H (m)	1000	1250	1500	1750	2000
2	d (m)	20	30	40	50	60
3	H (m)	40	60	80	100	120
4	H (m)	0.250	0.375	0.500	0.625	0.750
5	t (m)	1.5	2.5	3.5	4.5	5.5
	E (GPa)	6.0	7.5	9.0	10.5	12.0
6	E' (GPa)	6.0	7.5	9.0	10.5	12.0
	E_s (GPa)	4.0	5.0	6.0	7.0	8.0
	E (GPa)	3.750	5.625	7.500	9.375	11.250
7	E' (GPa)	3.750	5.625	7.500	9.375	11.250
	E_s (GPa)	5.000	5.000	5.000	5.000	5.000
	E (GPa)	7.5	7.5	7.5	7.5	7.5
8	E' (GPa)	7.5	6.0	4.5	3.0	1.5
	E_s (GPa)	5.0	5.0	5.0	5.0	5.0

Table 2: Experimental values of the radial pressure coefficient.

Number	Radial pressure coefficient M					Variation coefficient (%)
1	1.461	1.463	1.464	1.465	1.465	0.118
2	1.461	1.492	1.496	1.485	1.466	1.059
3	1.423	1.461	1.472	1.474	1.473	1.491
4	1.425	1.453	1.461	1.455	1.429	1.139
5	1.510	1.431	1.374	1.330	1.294	6.144
6	1.496	1.496	1.496	1.496	1.496	0.006
7	1.254	1.385	1.496	1.592	1.676	11.254
8	1.496	1.409	1.309	1.194	1.058	13.388

$$\omega_{max} \le \frac{t}{5}, \tag{8}$$

where a is the radius of the interlayer and ω_{max} is the maximum deflection.

Under the action of the vertical uniformly distributed load q, the deflection of the circular thin plate can be calculated as

$$\omega = \frac{qa^4}{64D}\left(1 - \frac{r^2}{a^2}\right)^2, \tag{9}$$

where D is the bending stiffness given as $D = (Et^3)/(12(1-\mu^2))$, in which μ is Poisson's ratio.

Equation (8) can be written in the form of Equation (10) based on Equations (2) and (9):

$$\frac{3(1-\mu^2)(\gamma_m - \gamma_b)a^4}{16Et^3} \le \frac{1}{5}. \tag{10}$$

Therefore, it is feasible to use the superposition method if Equations (7) and (10) are satisfied, the mezzanine has a small deflection curve, and the neutral plane is considered as a plane.

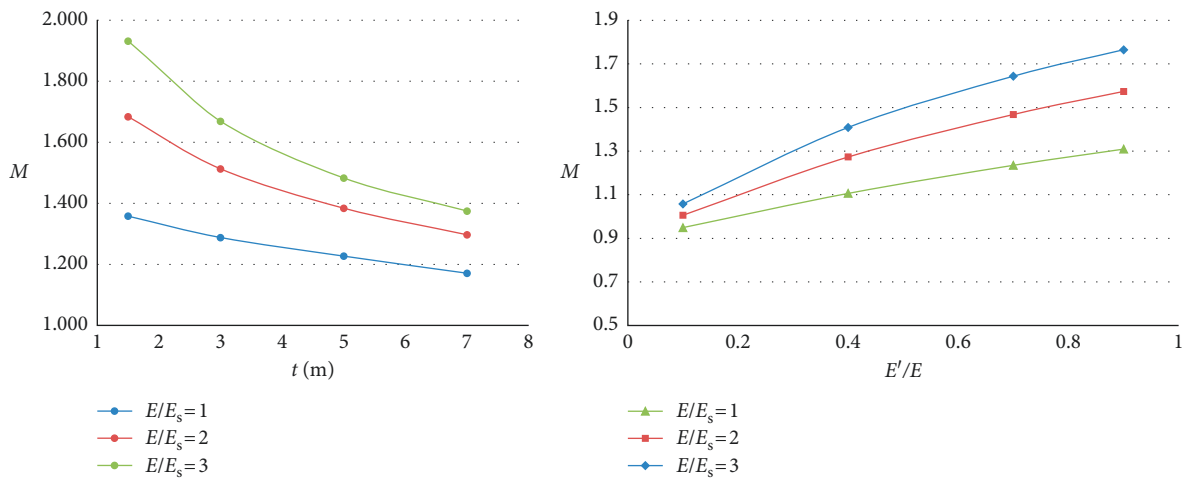

Figure 3: Fitting effect of the radial pressure coefficient: (a) elastic modulus ratio $E'/E = 1$ m; (b) interlayer thickness $t = 2$ m.

In a circular thin plate, the relationship between the stress component and internal force is

$$\left.\begin{aligned} \sigma_r &= \frac{12M_r}{t^3}z, \\ \sigma_\theta &= \frac{12M_\theta}{t^3}z, \\ \tau_{r\theta} &= \frac{12M_{r\theta}}{t^3}z, \\ \tau_{\theta z} &= \frac{6Q_\theta}{t^3}\left(\frac{t^2}{4} - z^2\right), \\ \tau_{rz} &= \frac{6Q_r}{t^3}\left(\frac{t^2}{4} - z^2\right). \end{aligned}\right\} \tag{11}$$

For the axisymmetric bending, the relationship between the internal force and deflection is

$$\left.\begin{aligned} M_r &= -D\left(\frac{d^2\omega}{dr^2} + \mu\frac{1}{r}\frac{d\omega}{dr}\right), \\ M_\theta &= -D\left(\frac{1}{r}\frac{d\omega}{dr} + \mu\frac{d^2\omega}{dr^2}\right), \\ M_{r\theta} &= Q_\theta = 0, \\ Q_r &= -\frac{qr}{2}. \end{aligned}\right\} \tag{12}$$

Substituting Equations (2) and (9) into Equations (11) and (12), we get

$$\left.\begin{aligned} \sigma_r^{(ii)} &= \frac{3(\gamma_m - \gamma_b)}{4t^2}\left[(1+\mu)a^2 - (3+\mu)r^2\right]z, \\ \sigma_\theta^{(ii)} &= \frac{3(\gamma_m - \gamma_b)}{4t^2}\left[(1+\mu)a^2 - (1+3\mu)r^2\right]z, \\ \tau_{rz}^{(ii)} &= \frac{3(\gamma_m - \gamma_b)}{t^2}\left(z^2 - \frac{t^2}{4}\right)r, \\ \tau_{r\theta}^{(ii)} &= \tau_{\theta z}^{(ii)} = 0. \end{aligned}\right\} \tag{13}$$

The equilibrium equation of the axisymmetric problem is

$$\frac{\partial\sigma_z}{\partial z} + \frac{\partial\tau_{rz}}{\partial r} + \frac{\tau_{rz}}{r} = 0. \tag{14}$$

Substituting $\tau_{rz}^{(ii)}$ given in Equation (13) into the above formula yields

$$\sigma_z^{(ii)} = -2(\gamma_m - \gamma_b)\left(\frac{1}{2} - \frac{z}{t}\right)^2(t+z). \tag{15}$$

Therefore, it can be ignored because the values of $\tau_{rz}^{(ii)}$ and $\sigma_z^{(ii)}$ are small.

Substituting Equations (6) and (13) into Equation (5), the interlayer stress can be given as follows:

$$\left.\begin{aligned} \sigma_r &= -M\gamma_0 H + \frac{3(\gamma_m - \gamma_b)}{4t^2}\left[(1+\mu)a^2 - (3+\mu)r^2\right]z, \\ \sigma_\theta &= -M\gamma_0 H + \frac{3(\gamma_m - \gamma_b)}{4t^2}\left[(1+\mu)a^2 - (1+3\mu)r^2\right]z, \\ \sigma_z &= -\gamma_b H. \end{aligned}\right\} \tag{16}$$

where τ_{rz}, $\tau_{r\theta}$, and $\tau_{z\theta}$ are all equal to zero so that σ_r, σ_θ, and σ_z are the three principal stresses of the interlayer. Furthermore, σ_z is equal throughout the interlayer.

The minimum and maximum values of σ_r and σ_θ are obtained from the center and edge of the top and bottom surfaces of the interlayer, whose positions are represented as ($r=0$, $z=-t/2$), ($r=0$, $z=t/2$), ($r=a$, $z=-t/2$), and ($r=a$, $z=t/2$).

Comparing the maximum values in the latter and previous parts yields

$$\frac{3(\gamma_m-\gamma_b)a^2}{4tM\gamma_0 H}<0.05. \tag{17}$$

When the value of the ratio is small, it implies that the bending effect is not significant, and then the stress on the interlayer is calculated directly according to Equation (6). In addition, if Equation (7) is not satisfied, which implies that the interlayer is not a thin plate, then it can also be calculated according to Equation (6) when the vertical uniformly distributed load q is small and mainly the stress on the interlayer is considered.

In conclusion, the radial pressure coefficient has a significant impact on the interlayer stress. Moreover, the effects of a large radius ratio on the deformation and stress of the interlayer are initially considered in Equations (7), (10), and (17).

2.3. Critical Length of Interlayer. The critical radius of the interlayer is the maximum radius when it begins to collapse [24]. The interlayer collapse can be classified into two categories according to the mechanics: stability conditions and strength criteria. Therefore, the failure modes are also correspondingly classified into these two categories and are further divided into four types: buckling instability, bending instability, tensile failure, and shear failure. The critical radius of the interlayer, a_1–a_4, can be calculated from the stability condition or strength criterion at the beginning of the failure mode. First, the relevant mechanisms and patterns come into effect while the value of a is small.

Therefore, the critical length of the interlayer is

$$d_{cr}=2\min(a_1,a_2,a_3,a_4). \tag{18}$$

Equation (18) considers numerous mechanisms of interlayer collapse and compares the possibility of each mechanism with the radius.

The process of a_1–a_4 calculation in the failure mode of the interlayer is as follows:

(1) Buckling instability of the interlayer

Based on the radial buckling instability of the circular plate, the radial pressure of the sandwich edge is at least

$$M\gamma_0 H=\frac{1.224E}{1-\mu^2}\left(\frac{t}{a}\right)^2. \tag{19}$$

The radius of the interlayer is

Table 3: Physical and mechanical characteristics of rock.

Type of rock	ρ (kg·m^{-3})	E (GPa)	μ	c (MPa)	φ (°)	σ_t (MPa)
Interlayer	2500	4.28	0.205	1.2	32	0.6
Rock salt	2200	3.60	0.282	1.0	40	0.4

$$a_1=t\left[\frac{1.224E}{(1-\mu^2)M\gamma_0 H}\right]^{1/2}. \tag{20}$$

(2) Bending instability of the interlayer

When both sides of Equation (10) are equal, the deflection is large and the radius is

$$a_2=\left[\frac{16Et^3}{15(1-\mu^2)(\gamma_m-\gamma_b)}\right]^{1/4}. \tag{21}$$

(3) Tensile failure of the interlayer

The maximum tensile stress criterion is

$$\sigma_3-\sigma_t=0, \tag{22}$$

where σ_t is the tensile strength.

It is found that the tensile failure is most likely to occur along the radial direction of the top edge of the interlayer, and the radius of the interlayer is

$$a_3=\sqrt{\frac{4t(M\gamma_0 H+\sigma_t)}{3(\gamma_m-\gamma_b)}}. \tag{23}$$

(4) Shear failure of the interlayer

The Mohr–Coulomb criterion expressed by the principal stress is

$$\sigma_1-\sigma_3\frac{1+\sin\varphi}{1-\sin\varphi}+c\frac{2\cos\varphi}{1-\sin\varphi}=0, \tag{24}$$

where c is the cohesion and φ is the internal friction angle.

Similarly, σ_1 and σ_3 of the four types of locations are calculated, and it is found that the shear failure occurs first at the edge of the bottom surface of the interlayer. The principal stress at the bottom edge of the interlayer is

$$\left.\begin{aligned}\sigma_1&=-M\gamma_0 H-\frac{3(\gamma_m-\gamma_b)}{4t}a^2,\\ \sigma_3&=-\gamma_b H.\end{aligned}\right\} \tag{25}$$

Substituting the above equation into Equation (24) yields the radius of the interlayer as

$$a_4=\left[\frac{4t}{3(\gamma_m-\gamma_b)}\right]^{1/2}\cdot\left[\gamma_b H\frac{1+\sin\varphi}{1-\sin\varphi}+c\frac{2\cos\varphi}{1-\sin\varphi}-M\gamma_0 H\right]^{1/2}. \tag{26}$$

In addition, the rock salt interlayer is softened by the brine, and accordingly, its various parameters would change.

Table 4: Critical length of each interlayer under different conditions.

Number	H (m)	γ_b (N/m^3)	M	t (m)	E'/E	E/E_s	a_1 (m)	a_2 (m)	a_3 (m)	a_4 (m)
A1	950	9800	1.29	3.8	1.0	1.2	54.61	33.36	25.49	14.06
A2	965	10780	1.27	2.2	0.9	1.2	31.61	22.17	19.44	12.82
B	970	10780	1.27	4.0	1.0	1.2	55.60	70.00	110.00	74.00
C1	1020	9800	1.51	1.4	1.0	1.2	17.94	15.78	17.31	5.68
C2	1030	10780	1.32	2.8	0.9	1.2	38.20	26.56	23.07	14.10
C3	1050	11760	1.43	2.0	1.0	1.2	25.00	41.60	86.20	44.90

Table 5: Critical length and collapse condition of the interlayer (m).

Number	Design radius (L_1)	Critical radius (L_2)	Rest part length (L_3)	Unstable part length (L_4)	Logging length (L_5)	Accuracy $(\lvert L_5 - L_3\rvert)/L_3$ (%)
A1	20	14.06	5.94	14.06	6.5	90.6
A2	25	12.82	12.18	12.82	13.2	91.6
B	25	55.60	25	0	20	80
C1	20	5.68	2.96	17.04	3.2	91.9
C2	25	14.10	10.9	14.1	11.5	94.5
C3	20	25.00	20	0	20	100

It has been analyzed that both the elastic modulus E and radial pressure coefficient M decrease. The strength of the interlayer is reduced. In reference to the strength reduction method,

$$c' = \frac{c}{\lambda}, \qquad \tan\varphi' = \frac{\tan\varphi}{\lambda}, \tag{27}$$

where λ is the strength reduction factor and c' and φ' are the cohesion and internal friction angles after the interlayer is softened; the tensile strength σ_t is also reduced to σ_t'.

Simultaneously, Poisson's ratio of the interlayer is increased, which can be considered as follows:

$$A\left(\frac{E'}{E}\right)^n = \frac{0.5-\mu'}{0.5-\mu}, \tag{28}$$

where μ is Poisson's ratio after the interlayer is softened; parameters A and n can be fitted by the experimental data, and the values of the parameters are all set to 1.

Therefore, the calculation model of the critical radius of the interlayer involves the above formulas.

3. Application

To verify the mathematical model, the rock salt gas storage in Jintan, China, is simulated as an example. The Jintan storage project should be able to supply approximately 15 million standard cubic meters to the marketplace per day. To achieve this objective, a total of 57 rock salt caverns will be solution mined and six existing caverns will be recreated [25]. Technically, to ensure the overall stability of the gas storage, the average thickness of the rock salt available is approximately 140 m, with the depth ranging from approximately 900 to 1240 m underground.

According to the four critical radii of the above interlayer, we analyzed the interlayer collapse of the rock salt gas storage cavities and compared the calculated results with the field measurement results. The interlayers analyzed in this study originate from the three rock salt gas storage cavities in the Jintan area of China, which are labelled as A, B, and C. Among these, two interlayers are present in cavity A, one interlayer is in cavity B, and three interlayers are in cavity C.

The physical and mechanical characteristics of the interlayer and rock salt, as listed in Table 3, are based on the results of the previous experiments of rock mechanics conducted on the strata in this area.

The critical radius of each interlayer is calculated according to the established mathematical model. The basic characteristics of the interlayer and the results of the critical radius are listed in Tables 4 and 5, and the contrast between the calculation results and the actual measured data is shown in Figure 4.

It can be seen from Table 5 that the calculation results of the mathematical model established in this study have a high degree of accuracy with respect to the actual engineering results, and it is generally above 90%. From Figure 3, it is understood that the main factors affecting the interlayer collapse are the thickness and position of the interlayer, while different positions imply different concentrations of the brine. For example, interlayer A1 is thicker than interlayer A2; however, because of the low concentration of the brine at the position of interlayer A1, it is obvious that the interlayer is eroded by the brine. If there are weak parts or cracks in the interlayer, it would be easier for it to collapse and the logging length would be small.

For interlayer C3, although its thickness is small, the interlayer is at the bottom of the cavity where the brine concentration is nearly saturated, and the solubility of the interlayer is 0. So the destruction of the interlayer is very low, and it is difficult for the interlayer to collapse in this case.

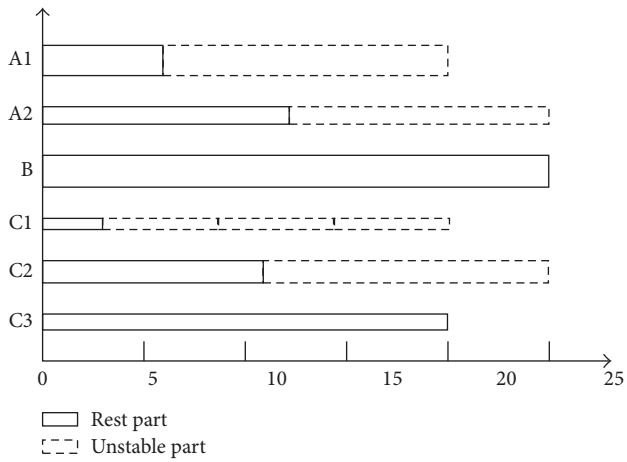

Figure 4: Collapse length of each interlayer.

Concurrently, because the thickness of interlayer B is large, it is not easy for it to collapse. However, in the process of cavity creation, the middle part of the interlayer is highly affected by the middle pipe and brine circulation, and a hollow is formed, of approximately 10 m in diameter. Thus, the accuracy of the collapse of interlayer B is low.

4. Conclusions

The main conclusions drawn from this study are as follows:

(1) This study defined the ratio of radial pressure to initial stress as the radial pressure coefficient, which makes the calculation of the interlayer stress simple and with satisfactory precision. This study considered the mechanical mechanism of the interlayer collapse in the proposed critical-length calculation model. This mathematical model comprehensively considered the strength and position of the interlayer and the concentration of brine, which is more suitable for an actual engineering problem.

(2) In general, the value of a_4 is smallest for most interlayers, which means the main form is shear failure of the interlayer collapse. The critical length of the interlayer is related to the position of the interlayer in the cavern. Because the concentration of brine is close to saturation, which has a little effect on the mechanical properties of interlayer characteristics, the instability of the interlayer is not easy.

(3) The critical-length calculation model has been used to analyze the collapse of numerous salt cavities in Jintan, China. It is demonstrated that the model has a high accuracy and can provide a good reference for the collapse of the interlayer. Therefore, it has significant relevance and practical application value for modelling the engineering method of rock salt gas storage.

Data Availability

The data used to support the findings of this study are included within the article.

Conflicts of Interest

The authors declare that they have no conflicts of interest regarding the publication of this paper.

Acknowledgments

The authors gratefully acknowledge the financial support provided by the National Natural Science Foundation of China (Grant No. 51174170) and China National Science and Technology Major Project (Grant No. 2017ZX05037001).

References

[1] X. L. Shi, Y. P. Li, C. H. Yang, D. A. Qu, H. J. Yang, and H. L. Ma, "Collapse control technology for interbeds in solution mining for oil/gas storage in multi-interbedded salt formation," *Chinese Journal of Geotechnical Engineering*, vol. 33, no. 12, pp. 1957–1963, 2011.

[2] L. Yu and J. J. Liu, "Stability of interbed for salt cavern gas storage in solution mining considering cusp displacement catastrophe theory," *Petroleum*, vol. 1, no. 1, pp. 82–90, 2015.

[3] G. Zhang, Y. Li, C. Yang, and J. J. K. Daemenet, "Stability and tightness evaluation of bedded rock salt formations for underground gas/oil storage," *Acta Geotechnica*, vol. 9, no. 1, pp. 161–179, 2014.

[4] W. Xing, J. Zhao, Z. M. Hou, P. Were, M. Y. Li, and G. Wang, "Horizontal natural gas caverns in thin-bedded rock salt formations," *Environmental Earth Sciences*, vol. 73, no. 11, pp. 6973–6985, 2015.

[5] K. Khaledi, E. Mahmoudi, M. Datcheva, and T. Schanz, "Stability and serviceability of underground energy storage caverns in rock salt subjected to mechanical cyclic loading," *International Journal of Rock Mechanics and Mining Sciences*, vol. 86, no. 1, pp. 115–131, 2016.

[6] T. T. Wang, H. L. Ma, C Yang, X. Shi, and J. J. K. Daemen, "Gas seepage around bedded salt cavern gas storage," *Journal of Natural Gas Science and Engineering*, vol. 26, no. 1, pp. 61–71, 2015.

[7] D. Park, D. Ryu, and B. Choi, "Numerical analysis-based shape design of underground rock caverns for thermal energy storage," *Rock Mechanics and Rock Engineering*, vol. 47, no. 6, pp. 2307–2312, 2014.

[8] L. Bojan, P. Jelušič, and D. Boumezerane, "The feasibility analysis of underground gas storage caverns," *Engineering Structures*, vol. 55, no. 1, pp. 16–25, 2013.

[9] L. J. Ma, H. F. Xu, M. Wang, and E. B. Li, "Numerical study of gas storage stability in bedded rock salt during the complete process of operating pressure runaway," *Chinese Journal of Rock Mechanics and Engineering*, vol. 2, no. 1, pp. 4108–4115, 2015.

[10] G. Wang, K. Guo, M. Christianson, and H. Konietzky, "Deformation characteristics of rock salt with mudstone interbeds surrounding gas and oil storage cavern," *International Journal of Rock Mechanics and Mining Sciences*, vol. 48, no. 6, pp. 871–877, 2011.

[11] W. G. Liu, Y. P. Li, C. H. Yang, J. J. K. Daemen, and D. Y. Jiang, "A new method of surface subsidence prediction for natural gas storage cavern in bedded rock salts," *Environmental Earth Sciences*, vol. 75, no. 9, pp. 1–17, 2016.

[12] Y. P. Li, X. L. Shi, C. H. Yang, and D. A. Qu, "Several key problems about control of solution mining for oil/gas storage in deep salt mine," *Chinese Journal of Rock Mechanics and Engineering*, vol. 31, no. 9, pp. 1785–1796, 2012.

[13] D. Y. Jiang, S. Ren, X. R. Liu, and B. X. Liu, "Stability analysis of rock salt cavern with catastrophe theory," *Rock and Soil Mechanics*, vol. 26, no. 7, pp. 1099–1103, 2005.

[14] R. Bekendam and W. Paar, "Induction of subsidence by brine removal," in *Proceedings of the SMRI Fall Meeting*, pp. 1–12, Rome, Italy, October 2002.

[15] X. L. Shi, Y. P. Li, C. H. Yang, D. A. Qu, and H. L. Ma, "Research on mechanical mechanism of interlayer collapse in solution mining for salt cavern gas storage," *Rock and Soil Mechanics*, vol. 30, no. 12, pp. 3615–3620, 2009.

[16] W. G. Liang, C. D. Zhang, H. B. Gao, S. G. Xu, and X. Q. Yang, "Experimental study of mechanical properties of gypsum saturated in brine," *Chinese Journal of Rock Mechanics and Engineering*, vol. 29, no. 6, pp. 1156–1163, 2010.

[17] G. C. Liang, M. Q. Wang, X. Y. Peng, and S. Zhang, "Numerical simulation of the creep deformation of underground salt cavern gas storages," *Natural Gas Industry*, vol. 34, no. 7, pp. 88–92, 2014.

[18] S. N. Moghadam, H. Mirzabozorg, and A. Noorzad, "Modeling time-dependent behavior of gas caverns in rock salt considering creep, dilatancy and failure," *Tunnelling and Underground Space Technology*, vol. 33, no. 1, pp. 171–185, 2013.

[19] G. Wang, W. Xing, J. F. Liu, Z. M. Zhou, and P. Were, "Influence of water-insoluble content on the short-term strength of bedded rock salt from three locations in China," *Environmental Earth Sciences*, vol. 73, no. 11, pp. 6951–6963, 2015.

[20] L. J. Ma, X. Y. Liu, S. N. Ma, and D. Wang, "Numerical analysis of in-situ ground stress in deep rock salt stratum containing mudstone inter-layers," *Journal of PLA University of Science and Technology*, vol. 10, no. 6, pp. 604–609, 2009.

[21] S. Ren, Y. J. Wen, D. Y. Jiang, J. Chen, D. A. Qu, and C. H. Yang, "Experimental research on softening in mudstone interlayer," *Rock and Soil Mechanics*, vol. 34, no. 11, pp. 3110–3116, 2013.

[22] L. J. Ma, X. Y. Liu, and M. Y. Wang, "Experimental investigation of the mechanical properties of rock salt under triaxial cyclic loading," *International Journal of Rock Mechanics and Mining Sciences*, vol. 62, no. 9, pp. 34–41, 2013.

[23] W. Liu, Y. P. Li, C. H. Yang, J. J. K. Daemen, Y. Yang, and G. M. Zhang, "Permeability characteristics of mudstone cap rock and interlayers in bedded salt formations and tightness assessment for underground gas storage caverns," *Engineering Geology*, vol. 193, no. 1, pp. 212–223, 2015.

[24] T. Meng, W. G. Liang, Y. D. Chen, and Y. J. Yu, "Theoretical analysis of periodic fracture for gypsum interlayer during construction of bedded salt cavern," *Chinese Journal of Rock Mechanics and Engineering*, vol. 34, pp. 3267–3273, 2015.

[25] X. L. Shi, W. Liu, J. Chen et al., "Geological feasibility of underground oil storage in Jintan salt mine of China," *Advances in Materials Science and Engineering*, vol. 2017, Article ID 3159152, 11 pages, 2017.